How much kinetic braiding does phantom dark energy require?

Local bounds for a cubic Galileon and a finite-window test on DESI DR2 expansion histories

Erno Pirinen
Independent researcher

28 November 2026

Abstract

Kinetic gravity braiding can stabilize a scalar field as its equation of state crosses $w = -1$. We ask how small its dimensionless braiding-to-gradient ratio can remain. For a minimally coupled scalar with $G_3 = \gamma X$, constant γ, and $G_{2X} \leq 0$, we derive $|\alpha_B|/(Dc_s^2) > 1/10$ at every stable epoch of nonnegative scalar enthalpy. The result is independent of the potential and includes the original kinetic-sign prior of the massive Galileon fit of Wolf, Ferreira and García-García. For a positive linear kinetic term, an exact rolling solution crosses $w = -1$ locally at a ratio below 0.04 with $c_s^2 = 47/19$. Separately, we test whether any regular braiding profile can meet a prescribed ratio cap along released general-relativistic expansion histories on $0 \leq z \leq 2$. In each of four DESI DR2 flat-CPL selections and two chain trims, at least 89.05% of phantom weight fails a cap of 0.06 irrespective of earlier evolution. At 0.08 a majority admits a profile on this window when the initial braiding is free. At a comparison cap of 0.04, exclusions cover at least 99.32% of phantom weight in every CPL sample and at least 98.61% in the corresponding smooth-bin samples. Without a CMB likelihood, phantom incidence across six fixed-knot fits ranges from about 69% to 95%. These finite-sample statements quantify compatibility conditional on the released expansion histories and on the stipulated cap.

1 Two ways to ask the question

A scalar with pressure p_ϕ and positive density ρ_ϕ has a phantom phase when $w_\phi = p_\phi/\rho_\phi < -1$. Kinetic mixing with the metric allows stable phantom evolution and smooth crossings of $w_\phi = -1$ in theories with one scalar degree of freedom [3]. The amount of mixing a crossing requires depends on the question being asked. An explicit Lagrangian ties the braiding to the scalar motion. A background expansion history inferred from observations supplies an enthalpy history, while leaving the braiding free.

We study these two situations with the same dimensionless ratio. In the Bellini–Sawicki convention [4], let $b = \alpha_B$, $D = \alpha_K + 3b^2/2$, and $q = Dc_s^2$. A positive kinetic coefficient and a positive squared scalar speed require $D, q > 0$. Write $r = |b|/q$ for the instantaneous ratio and R for a proposed upper bound on r. Throughout we assume spatial flatness, a constant positive reduced Planck mass M, minimally coupled external matter and luminal tensor propagation. We use $H > 0$, $N = \ln a$, $\epsilon = \dot{H}/H^2$, and $a = 1$ today. Cataneo and Koyama constructed stable, minimally coupled examples that cross the divide in a nonparametric scan and asked how additional restrictions on braiding would affect such solutions [10]. Vasilev et al. analyze wave-induced instabilities in the shift-symmetric class [11]. Linder relates crossing to the gravitational response within shift-symmetric Horndeski gravity [12]. Our background calculation quantifies the extra condition $|b| \leq Rq$ for specified histories, including histories that admit stable crossings when that condition is relaxed. A cap on $|b|/q$ and a cap on $|b|$ alone specify different tests.

2 A local bound for constant cubic coupling

Take the scalar Lagrangian $K(\phi, X) - G_3(\phi, X)\Box\phi$, with $G_3 = \gamma X$ and constant γ. In signature $(-,+,+,+)$, $v = \dot{\phi}$ gives $X = v^2/2$ on the homogeneous background. Define

$$b = \frac{\gamma v^3}{M^2 H}, \qquad u = \frac{2XK_X}{M^2H^2}, \qquad h = \frac{\rho_\phi + p_\phi}{M^2H^2}, \qquad J = \frac{\gamma v^2 \dot{v}}{M^2H^2}. \tag{1}$$

The published scalar stress tensor gives $h = u + 3b - J$ [3, 6]. Differentiating b gives $b_N = 3J - \epsilon b$, including at $v = 0$. With $e = (\rho_{\rm ext} + p_{\rm ext})/(M^2H^2)$, Raychaudhuri gives $-2\epsilon = h + e$. The scalar gradient numerator in the same convention is $q = (2 - b)(-\epsilon + b/2) + b_N - e$ [4]. Eliminating e and J yields

$$q = 3u + 10b - 2h - b^2/2. \tag{2}$$

Theorem 1. *At a regular epoch with $u \le 0$, $h \ge 0$ and $q > 0$, one has $b > 0$ and $r > 1/10$. More precisely, $h < 25$ and $r \ge (10 - 2\sqrt{h})^{-1}$.*

Proof. Positivity of the right side of (2) forces $b > 0$. The term $-b^2/2$ then gives $q < 10b$. Dividing (2) by b and using $b/2 + 2h/b \ge 2\sqrt{h}$ gives $0 < q/b \le 10 - 2\sqrt{h}$. □

Every positive-density crossing passes through $h = 0$. The theorem applies there and throughout any subsequent nonphantom phase while its hypotheses hold. For the overlap with the linear-plus-quadratic kinetic model, Eq. (2) can also be obtained directly by eliminating the scalar acceleration from the background and scalar-stability equations in Sec. III of Tsujikawa [8]. The potential-independent ratio inequality follows from this rewriting of published equations. It applies to the entire original prior $\alpha \in [-10, 0]$ of the fit with $K = \alpha X - V$ and $\gamma = -\beta/\Lambda_3^3$ [6], conditional on the epoch satisfying these hypotheses. No evaluation of a best-fit trajectory is needed. In the massless, high-wavenumber quasi-static limit of that model, $\mu_\infty = 1 + b^2/(2q)$ [6]. Equation (2) then gives $10r = \mu_\infty + (2h - 3u)/q \ge \mu_\infty$. Applying this refinement to draws from a fit would require h, u and μ_∞ at the same epoch of each draw.

Changing the kinetic sign. A later fit to the massive Galileon allowed $\alpha > 0$ [7]. At a rolling point with $K = \alpha X - V$, $\alpha > 0$ and $h = 0$, one has $u > 0$ and $D = u + 6b + 3b^2/2$. If one additionally requires $c_s^2 \le 1$, then $q \le D$. Equation (2) gives

$$0 < u \le b^2 - 2b, \qquad 0 < q \le (5/2)b^2 + 4b. \tag{3}$$

The first inequality excludes $0 \le b \le 2$ and the second excludes $-8/5 \le b \le 0$. On the regular branch $b < 2$, put $B = -b > 8/5$. The ratio satisfies $r \ge 2/(5B - 8)$, so a cap of 0.04 requires $b \le -11.6$. This argument assumes a linear kinetic term and the extra speed ceiling.

A local solution illustrates how much that ceiling matters. In units $M = H(t_0) = 1$, take pressureless dust with $\rho_m(t_0) = 9/10$, $\alpha = v(t_0) = 1$, $\gamma = 1/10$, $\phi(t_0) = -520/4913$, and $V = m^2\phi^2/2$ with $m^2 = 24137569/104000$. Friedmann gives $\rho_\phi = 21/10$. The Raychaudhuri and scalar equations form a linear system for $(\dot{H}, \dot{v})$ with determinant $323/100$ in the normalization supplied in the repository. At t_0 the solution has

$$h = 0, \quad \dot{h} = 2448691/88400 > 0, \quad b = 1/10, \quad D = 323/200, \quad q = 799/200.$$

Thus $r = 20/799 < 0.04$ and $c_s^2 = 47/19 > 1$. Here $s = \dot{v}/(Hv) = 13$. More generally, at a rolling $h = 0$ point with $b > 0$, eliminating $u = b(s - 3)$ gives $s = (1/r - 1 + b/2)/3$ and $c_s^2 = 3/[1 + (8 + 5b)r]$. Thus $r \le 0.04$ on $0 < b < 2$ requires $s > 8$ and $c_s^2 > 1.74$. Smoothness and the nonsingular system give a local solution through the point. Conservation preserves the Friedmann constraint. Transversality gives a phantom-to-nonphantom crossing, and the strict stability and ratio inequalities persist on an open interval around it. This example establishes local existence. Its initial data were constructed algebraically and carry no observational weight.

3 Testing an expansion history with free braiding

For a prescribed effective dark-energy density and pressure, keep $h = (\rho_{\rm DE} + p_{\rm DE})/(M^2H^2)$. The same perturbation and Friedmann equations give the identity

$$q = b_N + (1+\epsilon)b - b^2/2 + h. \tag{4}$$

Only the constant-cubic model fixed b_N in terms of a scalar-field trajectory. Here $b(N)$ is a free C^1 function. We ask whether there exists one with $q > 0$ and $|b| \le Rq$ everywhere on $N \in [-\ln 3, 0]$. Class U imposes $b < 2$, selecting the branch below the braiding singularity. Class C1 also imposes $|b| \le 1$. The initial and final values are free within the specified amplitude class. A feasible profile satisfies a background-level scalar stability test with freely choosable positive D. Constructing a covariant theory that realizes it, propagating perturbations, and refitting a likelihood are further tasks.

For completeness, set $\theta = \arctan b$. The cap implies $\theta_N \ge G$, where

$$G = \tfrac{1}{2}\sin^2\theta + |\sin\theta|\cos\theta/R - (1+\epsilon)\sin\theta\cos\theta - h\cos^2\theta. \tag{5}$$

An exclusion certificate starts a lower comparison trajectory at or below the lowest admissible angle. On each cell its slope is strictly below a verified lower bound on G along that trajectory, so an admissible solution cannot cross it downwards. If the lower trajectory exceeds the upper angle, the cap is impossible. A compatibility certificate gives an explicit profile with strict positive margins on the entire interval. Strict margins suffice to certify the original weak cap, including $q > 0$. Unresolved rows keep their full weight. The calculations also use equivalent barriers or witnesses in b where convenient. Candidate profiles may be found in floating point. Their sign enters the certified counts only through the corresponding verified bounds.

In the CMB-anchored DESI chains we reconstruct the conserved dark-energy density from $w(a)$, with $X_{\rm DE}(a) = \exp[-3\int_1^a (1+w)\,\mathrm{d}\ln a]$. Thus $h = 3\Omega_{\rm DE,0}X_{\rm DE}(1+w)/E^2$ with $E = H/H_0$. The density left after subtracting baryons, cold dark matter and dark energy at $a = 1$ can include radiation and massive neutrinos. We use a separately conserved residual with $0 \le p_{\rm res} \le \rho_{\rm res}/3$. In units of today's critical density its contribution to E^2 lies between U_0a^{-3} and U_0a^{-4} for $a \le 1$, where U_0 is its present density fraction. Exclusions hold for every allowed residual. A compatibility witness in the grid comparison uses a common $b(N)$ for all those residuals. For the no-CMB flexknot fits the model background is flat dust plus dark energy.

4 What the finite grid establishes

We retain distinct posterior measures for each likelihood selection. A draw qualifies as phantom-bearing when $w < -1$ somewhere on $0 \le z \le 2$; this includes a draw that is phantom throughout the window. For a phantom-weight denominator W, certified excluded weight e_W and certified compatible weight c_W, the fraction excluded lies in $[e_W/W, 1 - c_W/W]$. These intervals account for unresolved classifications on the stored draws. Chain sampling error, prior choice, and uncertainty in the likelihood model have different meanings.

Flat CPL. We apply $w(a) = w_0 + w_a(1-a)$ to 356,578 physical chain rows across DESI DR2 BAO+CMB with Pantheon+, Union3, DESY5, or without supernovae [1]. T0 retains all physical rows and T30 drops the first $\lfloor 0.30\,n \rfloor$ physical rows in each chain before applying multiplicities. For a given row define the critical cap as the infimum of caps permitting a class-U profile. At $R = 0.06$, at least 89.05% of phantom weight is excluded in each of the eight selection/trim combinations. At $R = 0.08$, at least 53.03% is certified compatible in each. Monotonicity therefore brackets each weighted median critical cap in $[0.06, 0.08]$. The exclusion at 0.06 also rules out any longer trajectory with that cap and the same history on this window.

The compatibility at 0.08 leaves the initial braiding free at $z = 2$. The grid does not resolve an exact median or establish this interval for each row. At $R = 0.10$, imposing $|b| \leq 1$ leaves at least 74.42% excluded in every selection and trim. This is the highest cap tested for the CPL population.

Smooth bins and fixed knots. For the 523,321 physical DESI smooth-bin chain rows we use the published analytic transition formula in redshift, with $S_i(z) = [1+\tanh((z-z_i)/0.02)]/2$ [1]. The transition centers are $z_i = 0.7, 1.4, 2.1, 10$, with four free amplitudes and a final level fixed to $w_4 = -1$. The calculation evaluates the analytic reconstruction on released parameters. Replaying the historical Boltzmann-code interpolation would require its original table. Across the four CMB-anchored selections and both trims, 99.971–99.997% of the weight has a phantom episode. Independent amplitude draws from the nominal prior give approximately 87.50%; the corresponding prior after cosmological-solver viability cuts is unknown. In each selection and trim the lower endpoint of class-U exclusion at $R = 0.06$ exceeds its upper endpoint at $R = 0.08$ by at least 14.70 percentage points. At $R = 0.10$ class C1 excludes at least 89.12% in every smooth-bin selection and trim.

To study a different likelihood and parametrization, we use 166,449 distinct rows in six unpooled two- and three-knot reconstructions [2]. These piecewise-linear histories in a have separate likelihoods and priors from the DESI+CMB fits. Figure 1 shows the dependence of incidence on the supernova sample, with the nominal nested-sampling weights [9]. For BAO alone the two- and three-knot incidences are 94.72% and 94.43%. Adding Pantheon+ gives 68.79% and 70.38%, while adding DESY5 gives 86.76% and 86.20%. The unfiltered prior incidences are 86.30% and 91.72%, respectively. These comparisons change several assumptions simultaneously and do not isolate the effect of adding CMB data.

Define the total phantom duration by integrating $\mathrm{d}\ln a$ over all phantom segments of the window. Within each of the six fixed likelihood/knot-count pairs, split the phantom weight at $\frac{1}{2}\ln 3$, with equality in the long group. At class-U $R = 0.06$, the long group's excluded share exceeds the short group's by at least 65.00 percentage points in every pair. At $R = 0.04$, the signs of all six differences remain unresolved. A short observed segment can continue beyond $z = 2$. These are within-window associations and do not identify duration as the independent cause.

5 Interpreting a cap of 0.04

In an effective cubic theory, a passing gravitational wave can affect the scalar gradient terms. The criterion for onset of the classical instability depends on the wave strain and frequency, the braiding convention, and the validity of the effective theory at that frequency [5]. For the interaction in Eq. (2.14) of Creminelli et al. (2020), the wave parameter scales as $(\omega h_0^+/H)$ times the braiding-to-gradient ratio in their local effective action, with h_0^+ the wave strain. Its use for an evolving cosmological profile requires the local and cosmological scalar coefficients to match. The authors' cubic braiding coefficient equals $-b/2$. An illustrative coefficient magnitude 10^{-2} at $q = 1/2$ thus gives $r = 0.04$. Their discussion of massive black-hole binaries involves frequencies well below the example cutoff. Changing the wave changes the comparison, and extending it to more general operators requires their couplings as well [11]. Propagation across a source population and nonlinear evolution require further inputs. We use $R = 0.04$ as a numerical comparison point. No universal observed upper bound on r or observation of gravitational-wave decay enters this analysis.

At this comparison point class U excludes at least 99.32% of phantom weight in each CPL selection and trim. In Pantheon+ T30 the baseline calculation excludes 197,740 of 199,087 phantom-weight units, certifies 1,261 compatible, and leaves 86 unresolved. For smooth bins the corresponding floor across selections and trims is 98.61%. Its limiting sample, DESY5 T30, has

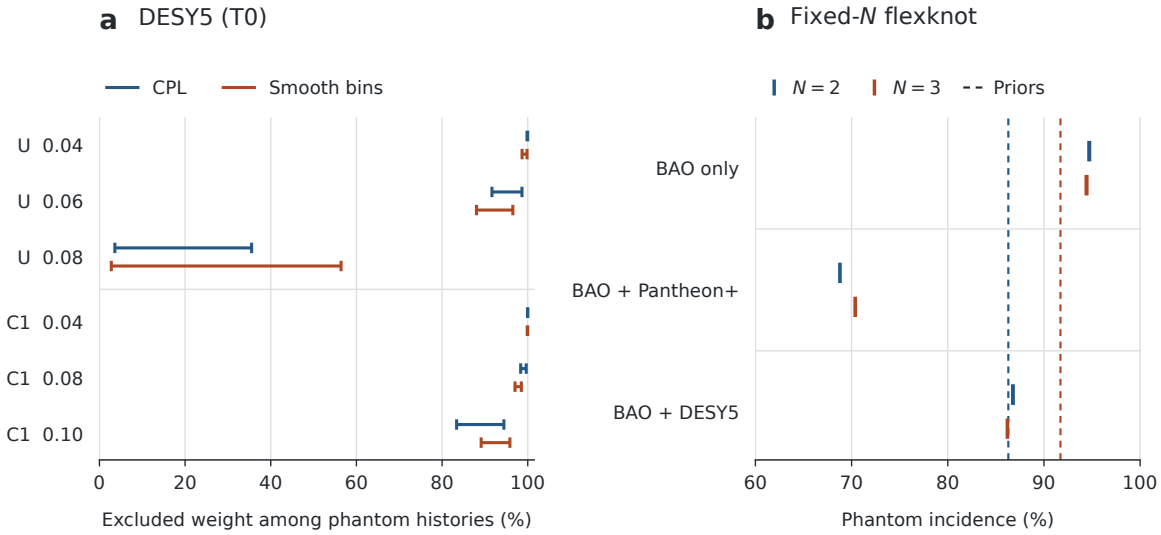

Figure 1: **Certified exclusion in matched CPL and smooth-bin cohorts, and phantom incidence in fixed-knot cohorts. a,** DESI DR2 BAO, CMB and DESY5 at T0, with no additional weight trim. Each segment spans the certified percentages of phantom posterior weight excluded at fixed Planck mass under the physical E-band. Within each fit's phantom population, the lower endpoint is the certified excluded fraction and the upper endpoint is one minus the certified compatible fraction. The CPL grid uses the common-profile sweep. Both fits share the likelihood selection and retain separate posterior measures. Labels give the amplitude class and the dimensionless ratio cap R in $|b_c| \leq Rq$. Class U imposes $b_c < 2$, and class C1 also imposes $|b_c| \leq 1$. **b,** Nominal weighted incidence of a phantom phase, $\min_{a\in[1/3,1]}(1+w(a)) < 0$, in each fixed-$N$ flexknot posterior. These BAO likelihood selections omit CMB. The upper and lower marks in each row represent $N = 2$ and $N = 3$, respectively. Dashed lines show the corresponding unfiltered priors. Incidence endpoint caps coincide at plot resolution. The intervals describe certificate coverage in panel a and numerical enclosure in panel b. Sampling uncertainty is a separate quantity. The accompanying data give the exact interval endpoints used in the plot.

289,052 phantom-weight units. One calculation certifies 285,036 excluded and an independent calculation certifies 544 compatible, giving a bracket of $[98.6106, 99.8118]\%$ rounded outward. Here we intersect cohort-level brackets. The flexknot duration comparison instead combines independently classified rows after checking for opposing signs, then evaluates both sets of classifications using the same stored nominal log weights.

Limitations. The exclusions follow from failing a necessary test on the stated interval. Restrictions of longer trajectories inherit this exclusion for the same history, cap and class. A positive witness can cease to extend when earlier times or additional endpoint conditions are imposed. The extent to which the median bracket moves on opening the window earlier remains unmeasured here. The duration split is also window-dependent. The chains were fitted under GR and a specified background model. A fit that varies gravity perturbations changes the likelihood through growth, lensing and the integrated Sachs–Wolfe effect. The percentages therefore describe a test on released draws. The explicit cubic theorem addresses a different object: a local implication for any trajectory in its model class. Combining those numbers into a probability for that model would require a new fit.

Reproduction and contributions. The accompanying reproduction repository includes hash-identified source-data manifests, row or cohort classification products, replay instructions, figure data and code, Lean proofs of specified algebraic implications, and exact symbolic checks of the local crossing. A claim-to-certificate index identifies the data, exact endpoints and replay commands for the numerical statements. Each replay guide distinguishes recounting certificates from recomputing inequalities on the original inputs. The covariant perturbation formula, background field equations, and applicability of the effective theory are physical inputs to these checks.

Erno Pirinen directed the project. AI systems carried out the mathematical derivations, literature searches, numerical work and writing. GPT-6.2 Astra coordinated the analysis, independently computed certificates and integrated the paper. Gemini 4 Neon developed independent certificate implementations, constructed the pure-quadratic crossing example and wrote the first draft. Claude Opus 5.5 checked the physical interpretation, independently derived the cubic bounds and tested comparison trajectories. Claude Fable 5.2 derived the enthalpy refinement and proposed the ratio sweep and window tests. Gemini feedback shared by the project director helped shape the public scope and interpretation. Computational and literature checks also used Codex research assistants. The paper is an AI-assisted preprint.

Data acknowledgments. This research used data obtained with the Dark Energy Spectroscopic Instrument (DESI). DESI construction and operations is managed by the Lawrence Berkeley National Laboratory. This material is based upon work supported by the U.S. Department of Energy, Office of Science, Office of High-Energy Physics, under Contract No. DE–AC02–05CH11231, and by the National Energy Research Scientific Computing Center, a DOE Office of Science User Facility under the same contract. Additional support for DESI was provided by the U.S. National Science Foundation (NSF), Division of Astronomical Sciences under Contract No. AST-0950945 to the NSF's National Optical-Infrared Astronomy Research Laboratory; the Science and Technology Facilities Council of the United Kingdom; the Gordon and Betty Moore Foundation; the Heising-Simons Foundation; the French Alternative Energies and Atomic Energy Commission (CEA); the National Council of Humanities, Science and Technology of Mexico (CONAHCYT); the Ministry of Science and Innovation of Spain (MICINN), and by the DESI Member Institutions: www.desi.lbl.gov/collaborating-institutions. The DESI collaboration is honored to be permitted to conduct scientific research on I'oligam Du'ag (Kitt Peak), a mountain with particular significance to the Tohono O'odham Nation. Any opinions, findings, and conclusions or recommendations expressed in this material are those of the author(s) and do not necessarily reflect the views of the U.S. National Science Foundation, the U.S. Department of Energy, or any of the listed funding agencies.

References

[1] M. Abdul Karim et al. (DESI Collaboration), "DESI DR2 results. II. Measurements of baryon acoustic oscillations and cosmological constraints", Phys. Rev. D **112**, 083515 (2025), doi:10.1103/tr6y-kpc6, arXiv:2503.14738; K. Lodha et al. (DESI Collaboration), "Extended dark energy analysis using DESI DR2 BAO measurements", Phys. Rev. D **112**, 083511 (2025), doi:10.1103/w4c6-1r5j, arXiv:2503.14743. DESI DR2 cosmology-chain release (2025).

[2] A. N. Ormondroyd, W. J. Handley, M. P. Hobson, and A. N. Lasenby, "Comparison of dynamical dark energy with ΛCDM in light of DESI DR2", Mon. Not. R. Astron. Soc. **547**, staf2207 (2026), doi:10.1093/mnras/staf2207, arXiv:2503.17342; A. Ormondroyd, "Nonparametric reconstructions of dynamical dark energy using flexknots", Zenodo dataset, version 2 (17 June 2025), doi:10.5281/zenodo.15681379.

[3] C. Deffayet, O. Pujolàs, I. Sawicki, and A. Vikman, "Imperfect dark energy from kinetic gravity braiding", JCAP **10** (2010) 026, doi:10.1088/1475-7516/2010/10/026, arXiv:1008.0048.

[4] E. Bellini and I. Sawicki, "Maximal freedom at minimum cost: linear large-scale structure in general modifications of gravity", JCAP **07** (2014) 050, doi:10.1088/1475-7516/2014/07/050, arXiv:1404.3713.

[5] P. Creminelli, M. Lewandowski, G. Tambalo, and F. Vernizzi, "Gravitational wave decay into dark energy", JCAP **12** (2018) 025, doi:10.1088/1475-7516/2018/12/025, arXiv:1809.03484; P. Creminelli, G. Tambalo, F. Vernizzi, and V. Yingcharoenrat, "Dark-energy instabilities induced by gravitational waves", JCAP **05** (2020) 002, doi:10.1088/1475-7516/2020/05/002, arXiv:1910.14035v2.

[6] W. J. Wolf, P. G. Ferreira, and C. García-García, "Cosmological constraints on Galileon dark energy with broken shift symmetry", Phys. Rev. D **113**, 023551 (2026), corrected by APS on 24 February 2026, doi:10.1103/bxvj-bsv1, arXiv:2509.17586v3.

[7] C. García-García, P. G. Ferreira, and W. J. Wolf, "The status of single scalar field dark energy", accepted in Phys. Rev. D (2026), doi:10.1103/jkcl-g4cq, arXiv:2607.07777v3.

[8] S. Tsujikawa, "Crossing the phantom divide in scalar-tensor and vector-tensor theories", Phys. Rev. D **113**, L041301 (2026), doi:10.1103/y858-4swl, arXiv:2508.17231v2.

[9] W. Handley, "`anesthetic`: nested sampling visualisation", J. Open Source Softw. **4**(37), 1414 (2019), doi:10.21105/joss.01414, arXiv:1905.04768. Software version 2.10.2, commit `b6076caf`.

[10] M. Cataneo and K. Koyama, "Non-parametric exploration of minimally coupled gravity with phantom crossing", Phys. Rev. D **113**, 122006 (2026), doi:10.1103/ckns-5ytv, arXiv:2512.13691v2.

[11] T. Borislavov Vasilev, M. Bouhmadi-López and P. Martín-Moruno, "Dark energy with a shift-symmetric scalar field: obstacles, loophole hunting and dead ends", arXiv:2406.12576v2 (2024).

[12] E. V. Linder, "Cosmology after Phantom Crossing by Horndeski Gravity", arXiv:2512.03139v2 (2025).